Valence and conduction band states of HfS_2: From bulk to a single layer

C. Kreis, S. Werth, R. Adelung, L. Kipp, and M. Skibowski
Institut für Experimentelle und Angewandte Physik, Universität Kiel, D-24118 Kiel, Germany

E. E. Krasovskii and W. Schattke
Institut für Theoretische Physik, Universität Kiel, D-24118 Kiel, Germany
(Received 3 October 2003; published 31 December 2003)

Electronic states of a material are intimately related to the dimension of the system. Epitaxial layers of transition metal dichalcogenides provide model systems in which the dimension can gradually be reduced by varying the film thickness. Applying combined angle-resolved photoemission and inverse photoemission on bulk HfS_2 and epitaxial layers of HfS_2 on WSe_2, we investigate the influence of the film thickness on two- and three-dimensional valence and conduction band states. While the direct band gap is observed to be independent of the thickness, the dispersion of states interacting perpendicularly to the layers is strongly affected as found from normal emission spectra with varying photon energy. The latter, a decreasing band width with decreasing number of layers, may be expected from general physical arguments, whereas the former appears to be rather surprising. However, both is confirmed by *ab initio* extended linear augmented plane wave $\mathbf{k}\cdot\mathbf{p}$ band structure calculations.

DOI: 10.1103/PhysRevB.68.235331 PACS number(s): 73.20.−r

I. INTRODUCTION

The layered transition metal dichalcogenides (TMDC's) constitute ideal materials to study the electronic structure of low-dimensional systems. Applying van der Waals epitaxy (VDWE),[1] well-defined films with a thickness of many down to a single sandwich layer can be grown to gradually decrease the dimension of the system. The TMDC's consist of a sequence of chalcogen-metal-chalcogen sandwich layers [Fig. 1(a)] with strong covalent and ionic bonding inside a sandwich separated by a van der Waals gap over which the sandwich layers only interact with weak van der Waals like forces. Due to this specific geometric structure, considerable anisotropies in optical and transport properties arise[2] and the TMDC's are usually described as quasi-two-dimensional materials. However, the electronic structure $E(\mathbf{k})$ does not exclusively consist of bands with two-dimensional (2D) character which only display large dispersion with surface-parallel wave vector $\mathbf{k}_\parallel$. Also bands with three-dimensional (3D) behavior are observed exhibiting $k_\perp$ dispersion perpendicular to the layers up to several eV[3] [A Brillouin zone and the corresponding $\mathbf{k}$ vectors of the TMDC $1T$-HfS_2 are depicted in Fig. 1(b).] These 3D bands originate from electronic states which interact across the van der Waals gap and are delocalized in the direction perpendicular to the layers. In ultrathin films of only a few sandwich layers these electronic states are substantially affected by the reduced dimension of the system. Consequently, fundamental properties of the TMDC's can change.

Recently, theoretical band structures calculations showed that the location of the valence band maximum of WSe_2 changes its position in $\mathbf{k}$ space from the Γ point of the Brillouin zone in the bulk crystal to the K point in one or two sandwich layers. Moreover, the computations predicted that the band gap considerably increases from bulk to ultrathin films.[4] Further calculations yielded that TiS_2 converts from a semimetal to a semiconductor if the film thickness is reduced from bulk to a few sandwich layers while $TiSe_2$ stays metallic from bulk down to one sandwich layer[5]. Experimentally, thin epitaxial films of layered materials have shown the localization of valence states between vacuum and substrate for, e.g., InSe,[6] SnS_2,[7] and WS_2 (Ref. 8) each deposited on graphite. In particular, while the valence band maximum of bulk WS_2 was located at the Γ point of the Brillouin zone, the valence band maximum of a single sandwich layer WS_2 was determined at the K point.

Here we employ VDWE to grow ultrathin HfS_2 films of about 1 and 5 monolayers (ML)[9] on p-WSe_2 and study the influence of the film thickness on the electronic structure. HfS_2 is an n-type semiconductor exhibiting a fundamental indirect band gap of 2.85 eV and a direct band gap of 3.6 eV located at the Γ point.[10] While the direct band gap is ascertained between a valence and a conduction band of rather 2D character, occupied, and unoccupied bands with strong 3D behavior are also encountered at slightly lower and higher energies, respectively. This facilitates to investigate how electronic states both with 2D and 3D properties are affected in ultrathin HfS_2 films by the reduced dimension of the system.

Epitaxial HfS_2 is characterized by *in situ* scanning tunnel-

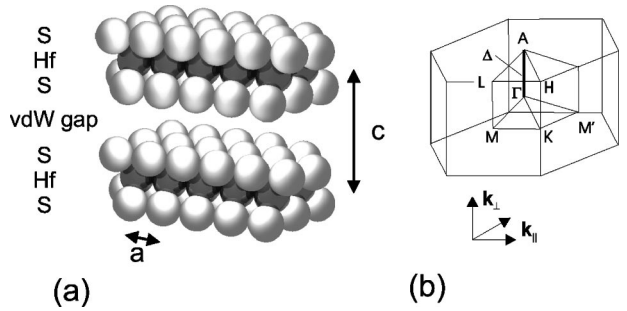

FIG. 1. (a) Schematic side view of the layered TMDC $1T$-HfS_2. (b) Brillouin zone of $1T$-HfS_2

ing microscopy (STM) and low-energy electron diffraction (LEED). Applying angle-resolved photoemission with synchrotron radiation and angle-resolved inverse photoemission using a grating spectrometer,[11] we consider the electronic structure $E(k_\perp)$ perpendicular to the layers. Combining both methods the occupied and unoccupied states are investigated on a common unique energy scale which allows us to determine the **k** resolved band gaps of ultrathin HfS_2 films with high precision.[12] *Ab-initio* band structure calculations employing the extended linear augmented plane wave method within the **k·p** formulation (ELAPW-**k·p**) (Ref. 13) corroborate the experimental work.

II. EXPERIMENTAL

All results described here were obtained on vacuum cleaved bulk samples and on clean HfS_2 monolayers epitaxially grown on air-cleaved and annealed WSe_2 bulk samples. Growth parameters (sulphur pressure $p_{S_2} \sim 2-3\times10^{-9}$ mbar, substrate temperatures $T_S = 600-650$ K, and a low hafnium flux) were chosen to yield a growth rate of about one monolayer HfS_2 per hour. Preparations were characterized employing *in situ* STM and LEED. Subsequently the samples were transported under ultra high vacuum conditions to the Hamburg Synchrotron Radiation Laboratory. Photoemission spectra were taken at the HONORMI beamline using our angular spectrometer for photoelectrons with high energy resolution ASPHERE.[14] An overall energy resolution of 50 meV$<\Delta E<$130 meV and angular resolution of $\Delta\vartheta<0.25°$ were chosen.

Inverse photoemission spectra were taken by using a compact grating spectrometer with parallel detection of photons in the energy range of 10 eV$<h\nu<$40 eV.[12] Electrons were focused on the sample by an Erdman-Zipf-type electron gun[15] with 1 mm^2 spot size and angle divergence $<3°$. Energy and momentum resolutions are typically 400 meV and 0.05 Å^{-1}.

In order to relate the energy scales of inverse and direct photoemission, we apply combined angle-resolved photoemission and inverse photoemission (CARPIP) spectroscopy.[12,16] In this technique a common energy scale for angle-resolved photoemission and inverse photoemission data is established by detecting the electron energy from the inverse photoemission electron gun with the photoemission electron energy analyzer. Thus a separate determination of the Fermi level as reference energy is avoided, and band bending does not affect the calibration. Therefore, this technique is predestined to very accurately determine energy differences between occupied and unoccupied states including **k** resolved band gaps.

III. BAND STRUCTURE CALCULATIONS

The calculations were performed with the extended linear augmented plane wave **k·p** method (ELAPW-**k·p**).[17,18] The self-consistent potential was constructed within the local density approximation (LDA) of the density functional theory with the full-potential augmented Fourier components technique described in Ref. 18.

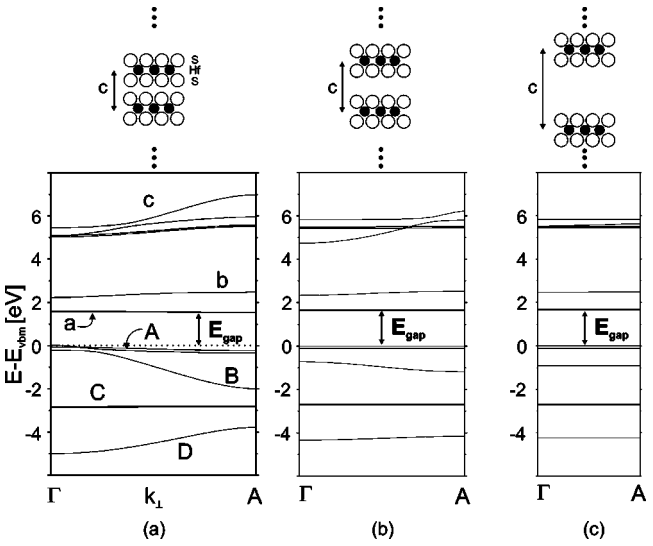

FIG. 2. Calculated band structure of HfS_2 with increasing size of the van der Waals gap. The in-plane lattice parameter is kept constant to the bulk value $a=3.635$ Å while the c axis is enlarged from (a) the bulk value $c=5.837$ Å to (b) $c=7.296$ Å and (c) $c=11.674$ Å. The direct band gap $E_{\rm gap}$ between the valence band maximum and band a is depicted for all three cases.

The Kohn-Sham equations were solved with the following computational setup: For the bulk HfS_2 crystal the basis set included 373 energy independent APWs (energy cutoff 13 Ry), and the extension of the radial basis set contributed another 124 basis functions. The extension was introduced following the prescriptions of Ref. 13. In the calculations with larger unit cells the computational parameters were changed so as to keep the same real space resolution of the APW basis set. The Brillouin zone (BZ) integrations were performed by the tetrahedron method with a mesh of 112 **k** points that divides the BZ into 6048 tetrahedra, 1437 of which are inequivalent.

IV. RESULTS AND DISCUSSION

To investigate how electronic states of HfS_2 are changed in ultrathin films, we first consider the calculated band structure of bulk HfS_2 which is depicted in Fig. 2(a) along the ΓA direction of the Brillouin zone, i.e., perpendicular to the surface. The unoccupied and occupied bands are denoted with small and capital letters, respectively. We can distinguish bands with either 2D character showing only slight $k_\perp$ dispersion (bands *b*, *a*, *A*, and *C*) or bands exhibiting 3D properties with a relatively large $k_\perp$ dispersion (bands *c*, *B*, and *D*). A Mulliken analysis of the corresponding electronic states can explain this difference. For example, band *A* originates from mainly S $3p_x$ and S $3p_y$ derived electronic states which are primarily localized inside the HfS_2 sandwich layers and show only little interlayer interaction. In contrast, band *B* is predominantly derived from S $3p_z$ orbitals which considerably interact across the van der Waals gap and thus are delocalized perpendicular to the layers.[19]

Hence, the band width along the ΓA direction greatly depends on the interlayer interaction. By increasing the van

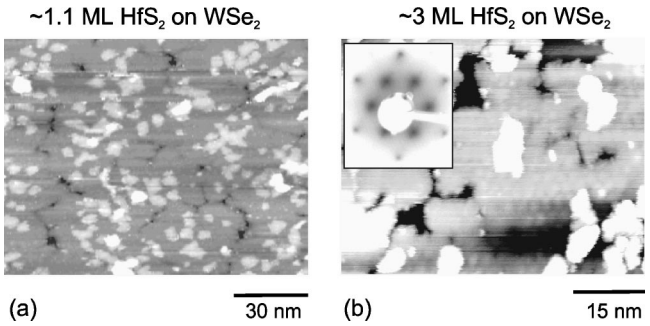

FIG. 3. Empty state STM pictures of (a) 1.1 ML and (b) 3 ML HfS_2 on WSe_2 [STM parameter: (a) 1.5 V bias, $I_t=0.2$ nA; (b) 2.3 V bias, $I_t=0.2$ nA]. (b) Corresponding LEED picture ($E_{\mathrm{kin}}=133$ eV).

der Waals gap in the calculation, the interaction between the layers is lowered and we are able to study how this affects the electronic structure. Figure 2(b) presents a calculation of bulk HfS_2 with a 25% enlarged van der Waals gap. The band width especially of the 3D bands *c*, *B*, and *D* is notably decreased, but they still display some $k_\perp$ dispersion due to a remaining interlayer interaction. Expanding the van der Waals gap by 100% results in completely flat bands [Fig. 2(c)].

While the 3D bands are significantly changed upon lowering the interlayer interaction, the 2D electronic states (bands *b*, *a*, *A*, and *C*) are only little affected. In particular, their binding energy is not altered and accordingly also their relative energy distance remains. This is crucial for the direct band gap E_{gap} which is ascertained between bands *A* and *a* with 2D character. The direct band gap E_{gap} is calculated to 1.55 eV. Although the computation underestimates the experimentally observed direct band gap of 3.6 eV (Ref. 10) because of the local density approximation,[20] the important fact for the discussion of ultrathin films constitutes that E_{gap} only increases by about 0.05 eV with larger van der Waals gap. Therefore, the direct band gap of a single HfS_2 sandwich layer should maintain the value of bulk HfS_2.

Experimentally, low-dimensional HfS_2 systems are realized by epitaxially growing ultrathin HfS_2 films on WSe_2 which are characterized by STM and LEED (Fig. 3). A smooth single sandwich layer HfS_2, shown in Fig. 3(a), is grown at substrate temperature $T_S=650$ K and a relatively low metal flux yielding an almost closed first layer and a second one which has just started with a coverage of only 10%. To fasten the preparation time, thicker films are prepared at higher metal flux and lower $T_S=600$ K. This results in slightly rougher epilayer surfaces with several unfinished sandwich layers displayed in Fig. 3(b) for three nominal monolayers (ML) HfS_2 on WSe_2.

The corresponding LEED picture of 3 ML HfS_2 is presented in the inset of Fig. 3(b). Due to surface sensitivity of LEED, only the epilayer contributes to the image which reveals the typical symmetry of the overlayer lattice and demonstrates the crystalline growth of HfS_2. Analyzing the diffraction pattern yields that epitaxial HfS_2 grows with its bulk in-plane lattice constant ($a_{\mathrm{HfS_2}}=3.635$ Å[3]) which is characteristic for VDWE.

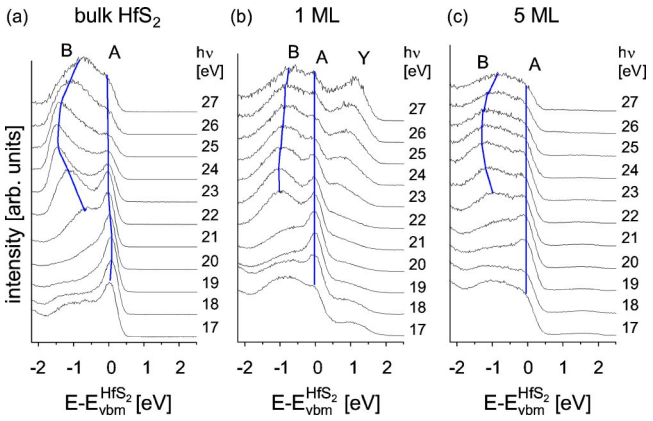

FIG. 4. Angle-resolved photoemission data (normal emission, $k_\parallel=0$) with various photon energies $h\nu$ of (a) bulk HfS_2, (b) 1 ML HfS_2/WSe_2, and (c) 5 ML HfS_2/WSe_2.

In order to experimentally study how 2D and 3D electronic states of bulk HfS_2 are changed in these ultrathin films, we exemplarily compare the upper two valence band emissions of bulk, 1 ML, and 5 ML HfS_2, shown in Fig. 4. Starting with bulk HfS_2, we consider the electronic valence structure $E(k_\perp)$ perpendicular to the surface applying angle-resolved photoelectron spectroscopy at normal emission with various photon energies $h\nu$ [Fig. 4(a)]. Assuming direct transitions between initial and final states, the $k_\perp$ component of the wave vector alters with the photon energy along the ΓA direction of the Brillouin zone. Two pronounced peaks denoted *A* and *B* are observed which are associated with the sulphur derived bands *A* and *B*, respectively [Fig. 2(a)]. The 2D and 3D character of the electronic states is manifested by the dissimilar $k_\perp$ dispersion. While the uppermost peak *A* only slightly changes its binding energy revealing 2D behavior, emission *B* clearly displays 3D properties with a relatively large $k_\perp$ dispersion of about 800 meV between photon energies $h\nu=21-27$ eV.

Figure 4(b) shows angle-resolved photoemission spectra of 1 ML HfS_2 on bulk WSe_2. Due to the surface sensitivity of ARPES mainly contributions of the HfS_2 layer are visible in the spectra. Only at higher photon energies a feature labeled *Y* located in the band gap of HfS_2 appears which is associated with WSe_2 derived states. Two HfS_2 related peaks labeled *A* and *B* are discernable and can be associated with the corresponding emissions *A* and *B* of bulk HfS_2 [Fig. 4(a)]. While structure *A* does not show any $k_\perp$ dispersion as expected from the band structure calculation [Fig. 2(c)], peak B still reveals a small but distinct dispersion of 250 meV. This dispersion is caused by the hybridization of overlapping S $3p_z$ orbitals of the epilayer and Se $4p_z$ orbitals of the WSe_2 substrate.[19]

With increasing thickness of the HfS_2 film, the electronic band structure along the ΓA direction starts to build up. To investigate this development, we have also taken photoelectron spectra of 5 ML HfS_2 between photon energies $h\nu=17$ eV-27 eV depicted in Fig. 4(c). At a film thickness of 5 ML HfS_2 only contributions of the epilayer are visible in the spectra and substrate emissions are completely suppressed. The two peaks labeled *A* and *B* are again visible and

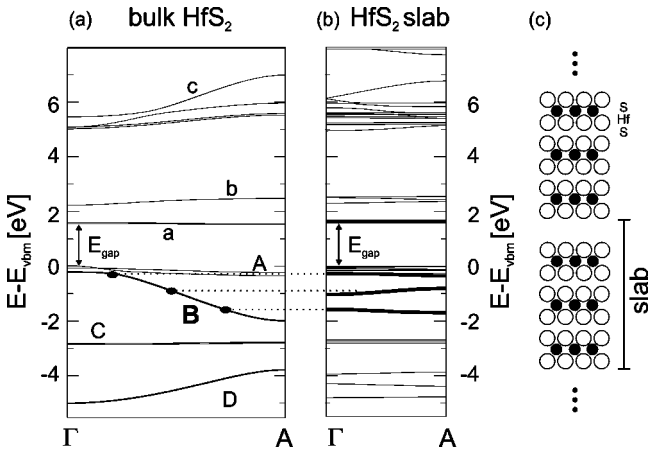

FIG. 5. Calculated band structure of (a) bulk HfS_2 and (b) slabs of three sandwich layers HfS_2. The bulk bands are split into three bands in the slab calculation. Exemplarily, three bands of the slab calculation (thick lines) are projected onto their corresponding bulk band *B* (dots). The direct band gap E_{gap} is depicted for both computations. (c) Schematic plot of the unit cell used in the slab calculation.

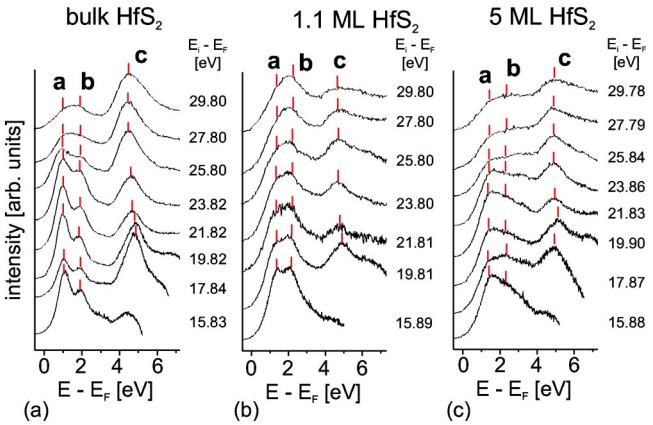

FIG. 6. Angle-resolved inverse photoelectron spectra with various initial electron energies E_i of (a) bulk HfS_2 and epitaxial HfS_2 films on WSe_2 with (b) 1.1 ML and (c) 5 ML thickness (normal incidence, $k_{\parallel}=0$, $E_F-E_{VBM}^{HfS_2}=2.6$ eV).

appear broadened because of the slightly increased roughness of the surface. Structure *A* still exhibits almost no dispersion. More significantly, the $k_{\perp}$ dispersion of emission *B* already amounts to 500 meV between photon energies $h\nu = 21-27$ eV indicating the evolution of the band structure along the ΓA direction. However, the dispersion of 500 meV is still smaller compared to the dispersion of 800 meV in the bulk.

To further elucidate the development of the band structure in ultrathin HfS_2 films, we compare band structure calculations of bulk HfS_2 [Fig. 5(a)] to computations of repeated slabs exemplarily containing three sandwich layers HfS_2 [Fig. 5(b)]. The unit cell of the slab calculation is constructed using bulk lattice parameters for the 3 HfS_2 layers separated to decrease the interaction between neighboring slabs by a vacuum region equal to a 25% stretched van der Waals gap [Fig. 5(c)]. Since three sandwich layers are contained in the unit cell in comparison with only one sandwich layer in the bulk unit cell, the number of bands has tripled [Fig. 5(b)]. The small remaining $k_{\perp}$ dispersion is due to a slight interaction of the electronic states over the vacuum region. Further increasing the vacuum region results in flat bands as shown above [Fig. 2(c)] but requires considerably more calculation time. The bulk bands with rather 3D character are each split into three, well separated bands in the slab calculation (e.g., bands *B* and *D*). On the other hand, each of the 2D bands (e.g., bands *A* and *C*) is also split into three bands but with only small energy separation. Moreover, they do not change their binding energy. Consequently, the direct band gap E_{gap} between bands *A* and *a* should remain constant also in films of several HfS_2 sandwich layers.

In contrast to the slab calculation, no periodicity perpendicular to the surface exists in an epitaxial film of 3 ML HfS_2. The electronic states possess only three $k_{\perp}$ values with discrete energies. Thus, we exemplarily project the three bands of the slab calculation plotted as thick lines [Fig. 5(b)] on the corresponding bulk band *B* displayed as dots [Fig. 5(a)]. Applying photoelectron spectroscopy in normal emission detects the different electronic states at dissimilar photon energies and the respective emission *B* exhibits dispersion [Fig. 4(c)]. It is interesting to note that the energy range covered by the three discrete energies is remarkably smaller than the band width of band *B*. The band structure along ΓA is not fully developed in ultrathin HfS_2 films. This explains the observed reduced dispersion of only 500 meV in 5 ML HfS_2 compared to 800 meV in bulk HfS_2.

Before we consider the direct band gap of ultrathin HfS_2 films, we explore the unoccupied electronic structure $E(k_{\perp})$ perpendicular to the surface employing angle-resolved inverse photoelectron spectroscopy at normal incidence with various initial electron energies E_i. Assuming direct transitions between initial and final states, the $k_{\perp}$ component of the electron wave vector is changed with E_i along the ΓA direction of the Brillouin zone. Figure 6 depicts spectra in the angle-resolved inverse constant initial energy spectroscopy mode of bulk HfS_2 and epitaxial HfS_2 films with 1.1 and 5 ML sandwich layers.

Starting with the conduction bands of bulk HfS_2, we find three emissions marked *a*, *b*, and *c* [Fig. 6(a)] related to the three corresponding groups of conduction bands [Fig. 2(a)] which are mainly derived from Hf 5*d* orbitals. While bands *a* and *b* exhibit 2D character with small dispersion, the group of bands *c* displays 3D behavior. As expected from the band structure calculation, emissions *a* and *b* only little vary their binding energy with changing $k_{\perp}$, while structure *c* exhibits $k_{\perp}$ dispersion of about 400 meV to lower energies with increasing initial electron energies E_i [Fig. 6(a)].

Figures 6(b) and 6(c) display inverse photoelectron data of 1.1 and 5 ML epitaxial HfS_2 on WSe_2, respectively. Due to the surface sensitivity of inverse photoemission, the spectra are governed by emission features of the epitaxial overlayer. In the epilayer spectra we observe three prominent peaks denoted *a*, *b*, and *c* which are related to the respective structures of bulk HfS_2. As in the photoemission spectra, the structures of 1 ML HfS_2 are less broadened than the corresponding features of 5 ML HfS_2 caused by the different sur-

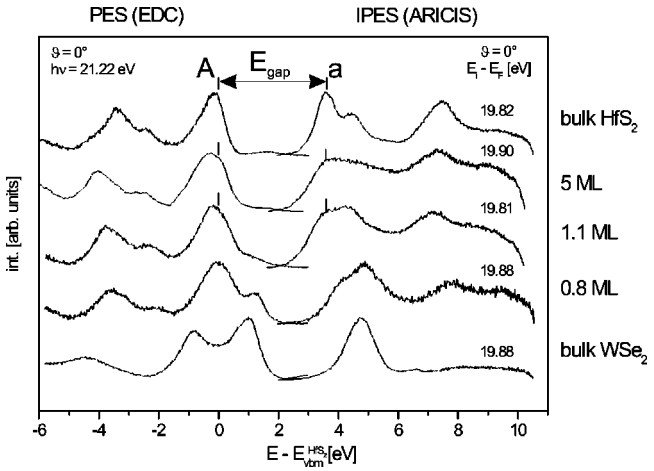

FIG. 7. Combined angle-resolved photoemission and inverse photoemission spectra of bulk WSe_2, 0.8, 1.1, and 5 monolayers epitaxial HfS_2 on WSe_2, and bulk HfS_2 showing the direct band gap E_{gap} at Γ of HfS_2 ($k_{\parallel}=0$).

face roughness of the epilayers. The emissions *a* and *b* of the epilayer show no $k_{\perp}$ dispersion as expected from the weakly dispersing structures of bulk HfS_2. Emission *c*, which changes its binding energy up to 400 meV with varying E_i in the bulk crystal, exhibits almost no dispersion in 1.1 ML and about 200 meV in 5 ML HfS_2 demonstrating the development of the unoccupied band structure with increasing film thickness.

To examine the direct band gap of epitaxial HfS_2 films, we apply combined angle-resolved photoemission and inverse photoemission (CARPIP) to study the occupied and unoccupied electronic structure on a common energy scale without using the Fermi level as a reference. This allows us to determine **k** resolved band gaps with high accuracy.[12,16] Figure 7 depicts CARPIP spectra of bulk WSe_2, HfS_2 on WSe_2 with increasing coverages ranging from 0.8 to 5 ML, and bulk HfS_2. The series of spectra nicely shows the transition of the emission features from pure bulk WSe_2 to HfS_2 related structures. The direct band gap E_{gap} of bulk HfS_2 has been determined by band mapping.[10] It amounts to 3.6 eV and is located between the valence band maximum and the lowest conduction band corresponding to peak *a*. Measuring the $k_{\perp}$ dispersion of the uppermost valence band emission *A* as in Fig. 4(a), the valence band maximum is detected at photon energy $h\nu=19$ eV corresponding to Γ where peak *A* exhibits the lowest binding energy. For epitaxial HfS_2 films with 1.1 and 5 ML thickness peaks *A* and *a* are clearly discernable. Since both structures do not show any $k_{\perp}$ dispersion, we can immediately determine the direct band gap at Γ to 3.6 eV$\pm$0.05 eV for 1.1 and 5 ML HfS_2. Obviously, the electronic states corresponding to emissions *a* and *A* and even their relative distance, i.e., the direct band gap at Γ, are only little affected in films with a thickness down to a single sandwich layer HfS_2 in excellent agreement with the band structure calculations shown in Figs. 2(c) and 5(b).

V. CONCLUSIONS

In summary, we applied combined angle-resolved photoemission and inverse photoemission together with band structure calculations to investigate the occupied and unoccupied electronic structure $E(k_{\perp})$ of ultrathin HfS_2 films. Regarding 3D electronic states, we found that the interlayer interaction determines the band width along the ΓA direction and found that the $k_{\perp}$ dispersion in 5 ML HfS_2 is still smaller compared to bulk HfS_2 due to an incomplete development of the band structure along ΓA. 2D bands were observed to remain their binding energy in ultrathin films. Consequently, the direct band gap, ascertained between 2D electronic states, maintains the bulk value of 3.6 eV for films with a thickness down to one sandwich layer of HfS_2 in good agreement with computed changes between band gaps of bulk and ultrathin HfS_2 films.

ACKNOWLEDGMENT

This work was supported in parts by BMBF Project No. 05 KS1 FKB and the Deutsche Forschungsgemeinschaft, Forschergruppe FOR 353.

[1] A. Koma, J. Cryst. Growth **201-202**, 236 (1999).
[2] J. Wilson and A. Yoffe, Adv. Phys. **18**, 193 (1969).
[3] R. Manzke and M. Skibowski, in *Electronic Structure of Solids*: *Photoemission and Related Data*, Vol. III/23b of *Landolt-Börnstein*, *New Series*, edited by A. Goldmann and E. Koch (Springer, Berlin, 1994).
[4] D. Voß, P. Krüger, A. Mazur, and J. Pollmann, Phys. Rev. B **60**, 14 311 (1999).
[5] C.M. Fang, R.A. de Groot, and C. Haas, Phys. Rev. B **56**, 4455 (1997).
[6] A. Klein, O. Lang, R. Schlaf, C. Pettenkofer, and W. Jaegermann, Phys. Rev. Lett. **80**, 361 (1998).
[7] W. Jaegermann, A. Klein, and C. Pettenkofer, in *Electron Spectroscopies Applied to Low-dimensional Structures*, Vol. 24 of *Physics and Chemistry of Materials with Low-Dimensional Structures* (Kluwer Academic Publishers, Dordrecht, 2000), p. 317.
[8] A. Klein, S. Tiefenbacher, V. Eyert, C. Pettenkofer, and W. Jaegermann, Phys. Rev. B **64**, 205416 (2001).
[9] A monolayer consists of one sandwich layer of chalcogen-metal-chalcogen.
[10] M. Traving, T. Seydel, L. Kipp, M. Skibowski, F. Starrost, E.E. Krasovskii, A. Perlov, and W. Schattke, Phys. Rev. B **63**, 035107 (2001).
[11] L. Kipp, M. Boehme, H. Carstensen, R. Claessen, and M. Skibowski, Rev. Sci. Instrum. **68**, 2144 (1997).
[12] M. Skibowski and L. Kipp, J. Electron Spectrosc. Relat. Phenom. **68**, 77 (1994).
[13] E.E. Krasovskii and W. Schattke, Phys. Rev. B **63**, 235112 (2001).

[14] K. Rossnagel, L. Kipp, M. Skibowski, and S. Harm, Nucl. Instrum. Methods Phys. Res. A **467-8**, 1485 (2001).
[15] P.W. Erdman and E.C. Zipf, Rev. Sci. Instrum. **53**, 225 (1982).
[16] H. Carstensen, R. Claessen, R. Manzke, and M. Skibowski, Phys. Rev. B **41**, 9880 (1990).
[17] E.E. Krasovskii and W. Schattke, Phys. Rev. B **56**, 12 874 (1997).
[18] E.E. Krasovskii, F. Starrost, and W. Schattke, Phys. Rev. B **59**, 10 504 (1999).
[19] C. Kreis, S. Werth, R. Adelung, L. Kipp, M. Skibowski, D. Voß, P. Krüger, A. Mazur, and J. Pollmann, Phys. Rev. B **65**, 153314 (2002).
[20] *Theory of the Inhomogeneous Electron Gas*, edited by S. Lundqvist and N. H. March (Plenum, New York, 1983), and references therein.